Localizing Metal Electrode from 3D Ultrasound Data Using RANSAC and Intensity Priors

M. Barva*, J. Kybic*, J.M. Mari**, C. Cachard** and V. Hlaváč*

* Center for Machine Perception, Czech Technical University in Prague, Prague, Czech Republic
** Centre de Recherche et d'Applications en Traitement de l'Image et du Signal, Institut National des Sciences Appliquées de Lyon, Lyon, France

barvam1@cmp.felk.cvut.cz

Abstract: In surgical interventions, miniature metallic tools such as thin electrodes and needles are introduced in tissue. Tracking systems are used to estimate their precise position. In this paper we describe an algorithm that exploits a three-dimensional ultrasound image and raw radio-frequency (RF) signal to determine the position of a thin, metallic electrode in biological tissue. We assume that electrode appears in 3D ultrasound image as a bright, elongated region. To estimate its position, a mathematical model of the region was established. It approximates the electrode axis with a polynomial curve. The voxel intensity distribution near the ray axis was determined from acquired RF signals. The model parameters are estimated by the RANSAC estimator. Finally, the electrode endpoints are located. The method was tested on real ultrasound data of a phantom with a thin tungsten electrode inserted. The results of experiments show that the method is stable even if the data are very noisy.

Introduction

During medical interventions, miniature surgical instruments such as needles and electrodes are introduced in biological tissue. In biopsy, for example, tissue samples are taken from a particular region of the body by means of a thin needle. Another example is the implantation of miniature electrodes into the cortex. All such cases require precise and fast determination of tool position inside the tissue structure.

The ultrasound imaging modality offers a non-invasive, not-expensive and portable way of data acquisition that can serve for automatic tool localization in biological tissue. Figure 1 and Figure 2 show an example of an image from the three-dimensional ultrasound scanner KRETZ Voluson 530D. It represents a biological tissue with a thin, tungsten electrode of 150 μm in diameter. In this paper we show how to estimate the positon of such object inside biological tissue. The processing of medical ultrasound data is difficult for several reasons. First, tissue is composed of a large number of particulars with the size comparable to the ultrasound wavelength, which act as scatterers giving rise to the typical speckle pattern. Second, many inhomogeneities present in the tissue are responsible for artifacts such as shades, reverberation and refractions. They cause objects to have missing parts and irregular contours. Third, volumetric data are very large.

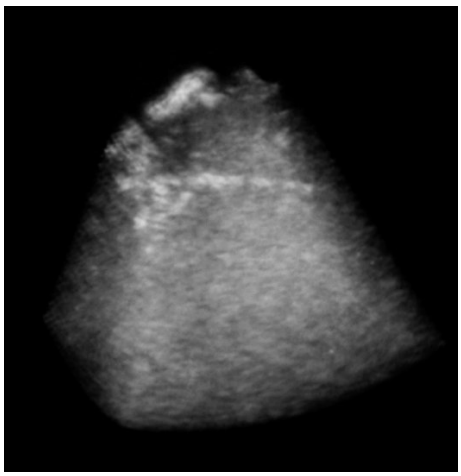

Figure 1: Three-dimensional ultrasound image of a tungsten electrode in a phantom mimicking biological tissue.

Existing methods

A variety of algorithms for object localization in three-dimensional images exists. Simple techniques detect boundaries between the object and the background. The boundaries are joined together to form the object contour. The main difficulty lies in a reliable detection of boundaries, especially in the case of noisy data. Techniques such as Canny detector [1] are likely to fail for ultrasound data. An adaptive model has been implemented [2]. It is based on a linear stochastic model of brightness intensity. For each voxel, its model parameters are estimated with the Bayes estimator. Although this technique makes the boundary detection robust, due to its high computational load, it is not suitable for applications where fast data processing is required. A set of elementary entities ("sticks") such as line-segments of the same length and different orientations can locally approximate the object contour [3]. The sticks algorithm assigns to each voxel a value equal to the maximum sum of voxel values along a stick over the set of sticks. Novotny [4] implemented an algorithm for electrode localization

ISSN: 1727-1983

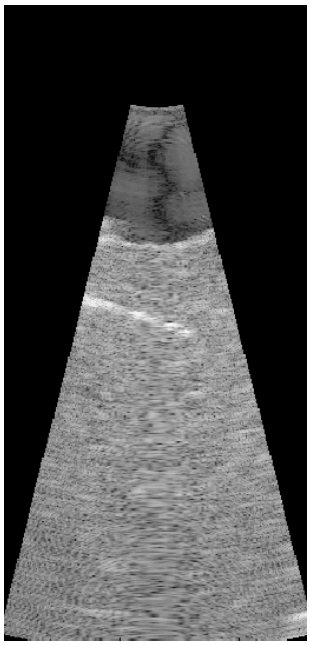

Figure 2: Planar cut of data (Figure 1) passing through the electrode axis.

in three-dimensional ultrasound data. Data are first segmented with thresholding. Next, they are divided into mutually disjoined regions. For each of them, the length and width is estimated with the PCA analysis. The region with the highest ration length/width is marked as the localized electrode. In [5], Ding demonstrated that a straight, elongated object can be localized with a parallel projection of the voxels. The projection area of the object is minimal when the direction of the projection is parallel with the electrode axis. Tao [6] introduced a model fitting algorithm to segment acoustical data. The object to localize is described with a superquadrics. Then the model parameters are estimated with the RANSAC estimator.

Proposed method

The method presented in this paper permits to determine the position of a thin, metallic electrode inside a biological tissue. Input data to the algorithm is a three-dimensional ultrasound image acquired from scanning the region of tissue comprising the electrode. Due to distinct acoustical properties of metal and tissue, the electrode voxels have in general higher values compared to tissue voxels. We suppose that the electrode diameter is very small (in order of hundreds of μm). It is likely to curve slightly as it penetrates the tissue. Therefore, we assume that the electrode presents itself in a 3D ultrasound image as a bright, elongated region with a curvilinear axis. To determine its position, we will use an algorithm similar to that proposed by Tao [6]. However, in our implementation the sought object is described with simpler mathematical model to reduce the computational cost. The electrode axis is modeled with a polynomial curve. We then use the fact that the voxel value depends on the distance from the axis. This dependence was experimentally established from measured radio-frequency (RF) signals. The model parameters are estimated by the RANSAC [7], which is an estimator known for its robustness against the noise. In the last step, the voxel values along the estimated electrode axis are used to determine its endpoints.

The next section describes in details the implemented method. In the section 4 we show the results of the algorithm on simulated and real ultrasound data. The paper concludes with a discussion of the algorithm properties and experiment results.

Method

The algorithm takes as input a 3D image described by a discrete function I,

$$I : A \mapsto B, \tag{1}$$

where $A = \{\mathbf{x}_i \in \mathbb{R}^3 \,|\, i = 1,2,\ldots,N\}$ is a countable set of points (voxels) and $B \subset \mathbb{R}_0^+$ is the set of voxel values. Output of the algorithm are parameters of a curve that approximates the electrode axis and two points on the curve determining the electrode tips.

Assumptions

Several assumptions have been made regarding the electrode appearance in the image. Due to distinct acoustical properties of metal and biological tissue, we assume that the electrode appears as a region $M \subset A$ in which the voxel values are much greater than the values of background voxels,

$$I(\mathbf{x}_i) \gg I(\mathbf{x}_j) \qquad \forall \mathbf{x}_i \in M, \forall \mathbf{x}_j \in A \setminus M. \tag{2}$$

Second, we expect that the length of the electrode visible in the data is typically much greater than its diameter. Taking into account possible curvature of the electrode, the region M can be modeled as the interior of a cylinder with a curvilinear axis.

Pre-segmentation

In the first step, the voxels from the set A are classified in two disjoined sets A_e and A_b. This operation roughly distinguishes between the electrode voxels and background voxels. It is accomplished by thresholding. The treshold is selected such that the set A_e consists of 10% of voxels with the highest values and $A_b = A \setminus A_e$. Figure 3 depicts the result of the pre-segmentation step. The goal is to accelerate the algorithm, since only the voxels from A_e are processed in the consecutive computations.

ISSN: 1727-1983

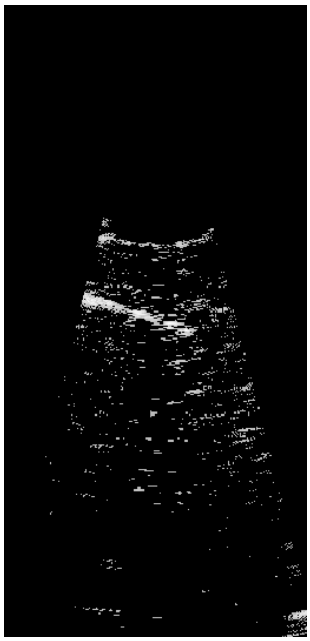

Figure 3: Pre-segmented data. Only the voxels from the set A_e are shown.

Model fitting

The presence of noise in the data causes that the set A_e contains also background voxels (false positives), see Figure 3. To distinguish them from electrode voxels, we implemented a model fitting approach. The electrode is described by a model with parameters estimated by the RANSAC algorithm.

Model The mathematical model of the electrode voxels is composed of two parts: (i) parametric polynomial approximates the curvilinear electrode axis, (ii) dependence between the voxel values and their distance from the electrode axis.

The localization algorithm takes into account possible electrode curvature in biological tissue. The electrode axis is modeled by a polynomial $l(t)$ with degree 3 defined as

$$\begin{aligned} l(t): x(t) &= a_0 + a_1 t + a_2 t^2 + a_3 t^3 \\ y(t) &= b_0 + b_1 t + b_2 t^2 + b_3 t^3 \\ z(t) &= c_0 + c_1 t + c_2 t^2 + c_3 t^3, \quad t \in \mathbb{R}, \end{aligned} \tag{3}$$

where $\Theta = (a_0, a_1, a_2, a_3, b_0, b_1, b_2, b_3, c_0, c_1, c_2, c_3)$ is the parameter vector determining the curve position and shape. The polynomial degree was set to 3 as the trade-off between the range of shape that can modeled with such a curve and undesirable ripples typical for higher-degree polynomials.

The values of electrode voxels in the region M vary. They depend on many aspects such as the acquisition geometry, the ultrasound probe, the energy profile of ultrasound beams, etc. To approximate this dependence, we experimentally estimated the function of voxel intensity on its distance from the electrode axis. Let $\{r_1(t), r_2(t), \ldots, r_M(t)\}$ be a set of backscattered RF signals corresponding to ultrasound beams passing through the electrode axis. Let $\{f_1(d), f_2(d), \ldots, f_M(d)\}$ be the set of their envelopes. In the Appendix we show how the envelope of a RF signal is calculated. For each $k = 1, 2, \ldots, M$, the signal $f_k(d)$ is shifted by a constant a_k,

$$g_k(d) = f_k(d - a_k), \tag{4}$$

so that g_k is a function of voxel intensity depending on its distance d from the electrode axis. The value a_k is determined using the cross-correlation function between the signals $\{f_1(d), f_2(d), \ldots, f_M(d)\}$.

We estimate the joint probability density function $p(v,d)$ between voxel intensity v and distance d. For fixed $d = d^*$ the $p(v,d^*)$ is estimated as a histogram of the values $\{g_1(d^*), g_2(d^*), \ldots, g_M(d^*)\}$. Figure 4 shows the resulting dependency between the voxel intensity and the distance d.

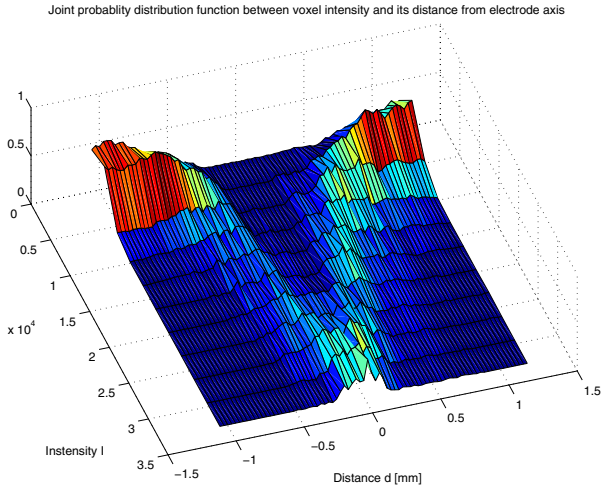

Figure 4: Estimated joint probability density function between voxel intensity and its distance from electrode axis.

We can now define the expectation

$$h(d) = \int_{-\infty}^{\infty} v p(v,d) \mathrm{d}v \tag{5}$$

This function is used to model the dependence between the voxel intensity and its distance from the electrode axis (Figure 5).

Estimation of parameter vector Θ The parameter vector Θ is estimated by the RANSAC algorithm [7]. It is a robust estimator used to fit models to data set with large number of outliers. The principle is simple: Repeatedly, small random subsets of the input data set are selected. Model is fitted to the subset and the quality of the estimated model is calculated using a cost function. The process terminates when the likelihood of finding a better model falls below a threshold.

In our application, we fit the polynomial curve with the parameter vector Θ to the data set A_e. Let $D \subset A_e$ be a set of randomly selected points from A_e. Since the

ISSN: 1727-1983

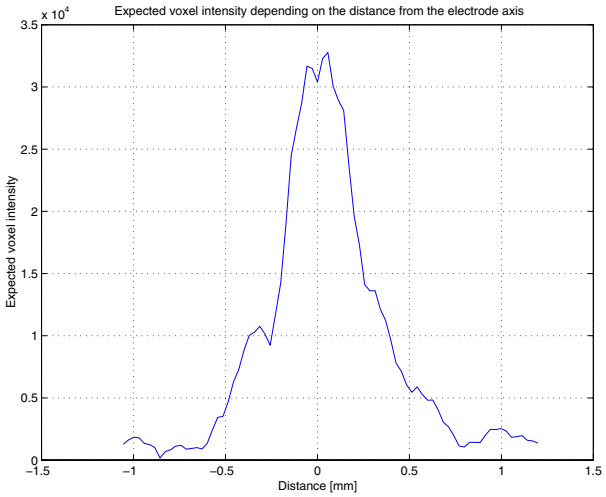

Figure 5: Expected voxel intensity as a function of the distance from the electrode axis.

number of parameters to estimate is 12 and each point in A_e has three coordinates, we set the size of D to 4. Once D is selected, the parameter vector Θ_k is calculated from (3) so that the polynomial passes through the points in D. To estimate the quality of the induced model $l_{\Theta_k}(t)$, the cost function $C(\Theta_k)$ is defined as

$$C(\Theta_k) = \sum_{\mathbf{x}\in A_e} [I(\mathbf{x}) - h(\varepsilon(l_{\Theta_k}(t),\mathbf{x}))]^2 \qquad (6)$$

where $\varepsilon(l_{\Theta_k}(t),\mathbf{x})$ is the distance of the point $\mathbf{x}$ from the curve $l_{\Theta_k}(t)$, $I(\mathbf{x})$ is the true intensity and $h(\varepsilon(l_{\Theta_k}(t),\mathbf{x}))$ is expected voxel intensity, see (5). The parameter vector $\hat{\Theta}$ that minimizes $C(\Theta_k)$,

$$\hat{\Theta} = \arg\min_{\Theta_k} C(\Theta_k) \qquad (7)$$

determines the polynomial curve that fits best the points from the data set A_e. The number of iterations is set to such a value that the probability of the event "better-than-currently-best estimated model is missed" is less than η. Setting η to 0.05 requires about 500 iterations. See [8] for details on how to set the number of iterations.

Algorithm - implemented estimation of the vector Θ with RANSAC.

- Input: Data set A_k.
- Output: Estimated parameter vector $\hat{\Theta}$.
- Iterations: $k := 0$, $\hat{\Theta} = \mathbf{0}$. Repeat steps 1-4 until $P\{\text{better solution exists}\} < \eta$.
  (1) $k := k+1$
  (2) Hypothesis generation
    (a) Select a random subset $D \subset A_e$, $|D| = 4$.
    (b) Compute Θ_k from (3).
  (3) Compute the cost function $C(\Theta_k)$ from (6).
  (4) Update model parameters: If $C(\hat{\Theta}) > C(\Theta_k)$, then $\hat{\Theta} := \Theta_k$.

Endpoint localization

The position of the electrode is determined by its endpoints. These points are located on the polynomial curve $l_{\hat{\Theta}}(t)$ that approximates the electrode axis. Let us define a function $a(t)$ by formula

$$a(t) = I(l_{\hat{\Theta}}(t)); \qquad \forall t \in \mathbb{R} : l_{\hat{\Theta}}(t) \in A. \qquad (8)$$

It is a function of voxel intensities along the curve $l_{\hat{\Theta}}(t)$, see Figure 6. The range of t values corresponding

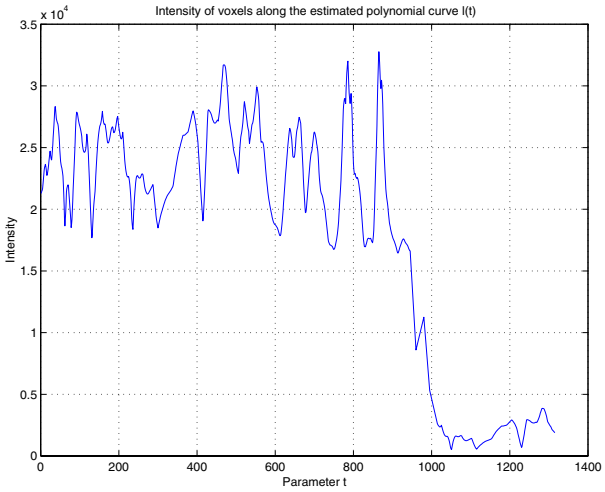

Figure 6: Voxel intensity along the estimated polynomial curve $l_{\hat{\Theta}}(t)$.

to the electrode should be now indentified .Two points on the curve $l_{\hat{\Theta}}(t)$ are marked as the endpoints if the value of the function $a(t)$ falls under given threshold T. Its value is determined from $p(i|electrode)$, resp. $p(i|background)$, which is the conditional probability of the intensity i given electrode voxel, resp. background voxel. Figure 5 shows that the radius of the region M is approximately 0.5 mm, so the values of the functions $\{g_1(d), g_2(d), \ldots, g_N(d)\}$ for $|d| \leq 0.5$ are the intensities of electrode voxels. Analogously, the values of the function $\{g_1(d), g_2(d), \ldots, g_N(d)\}$ for $|d| > 0.5$ are the intensities of background voxels. Their histograms were used to construct the probabilities $p(i|electrode)$ and $p(i|background)$ shown in Figure 7. Finally, the value of T is set to the point, where $p(i|electrode) = p(i|background)$. In our implementation T is approximately 12000.

Results

To test the algorithm, we used 3D ultrasound data form the ultrasound scanner KRETZ Voluson 530D. A tungsten electrode of 150 μm was inserted into a cryogel phantom mimicking the acoustical properties of biological tissue. The region of the phantom comprising the electrode was scanned with the scanner's transducer operating at 7.5 MHz. We acquired volumetric data of the size 680x680x1000 voxels. Figure 8 depicts the result

ISSN: 1727-1983

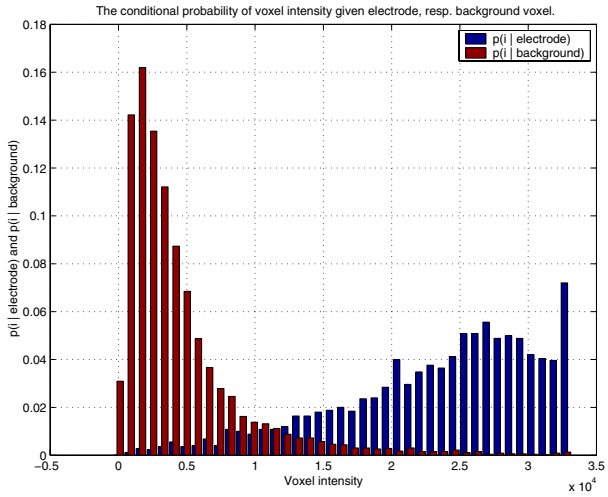

Figure 7: The conditional probability $p(i|electrode)$, resp. $p(i|background)$ of voxel intensity i given electrode, resp. background voxel.

of an experiment. The axis of the localized electrode is marked in green.

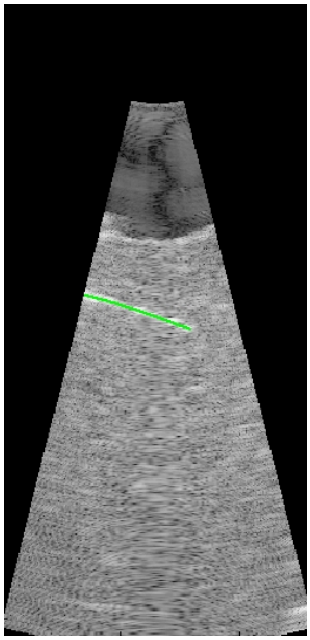

Figure 8: Result of the localizatin algorithm. Localized electrode is marked in green.

Conclusion

The ultrasound modality is widely used in many applications of medical diagnostics and research. One of them is the localization of miniature surgical instruments once they are inserted into biological tissue. To facilitate this task, we developed an algorithm capable of automatic localization of metallic electrode from volumetric ultrasound data. To surmount the problem of noise, a model fitting approach was adopted. The RANSAC estimator is used to estimate the model parameters. The algorithm was tested on 3D ultrasound data from the ultrasound scanner KRETZ Voluson 530D. The results of the experiments show that the method is stable even if the data contain high level of noise. Finally, the computational time is in order of seconds without any optimization permitting to achieve near real-time localization.

Acknowledgement

The 1st author was supported by The Grant Agency of the Czech Academy of Sciences under project 1ET101050403 and by the French Embassy under the project of doctoral studies with co-supervision. The 2nd author was supported by the The Czech Ministry of Education under project MSM6840770012.

Appendix

Bamber [9] and Dydenko [10] describe the ultrasound image formation from RF signals. The voxel intensity in an ultrasound image is defined by the envelope of RF signals. Let $r(t)$ be a RF signal. Figure 9 shows an example, where we can observe the ultrasound pulse reflection from the electrode.

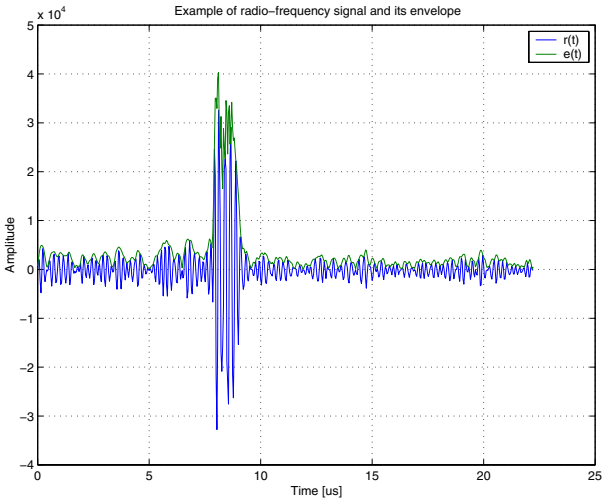

Figure 9: Example of a raw RF signal $r(t)$ and its envelope $e(t)$. The peak corresponds to the reflection of the ultrasound pulse from the electrode.

For the signal $r(t)$ its envelope $e(t)$ (Figure 9) is determined as the complex modulus of the analytic signal of $r(t)$,

$$e(t) = |r(t) + \mathrm{j}\hat{r}(t)| \tag{9}$$

where $\hat{r}(t)$ is the Hilbert transform of $r(t)$,

$$\hat{r}(t) = \frac{1}{t} * r(t). \tag{10}$$

The relation $f(d)$ between the voxel intensity and its distance d from the origin of the particular ultrasound

ISSN: 1727-1983

beam can be established as

$$f(d) = e\left(\frac{2d}{v}\right) \tag{11}$$

where v is the velocity of sound in the medium.

References

[1] R. C. Gonzales and R. E. Woods. *Digital Image Processing*. Addison-Wesley, 1993.

[2] A. D. Santis and C. Sinisgalli. Bayesian approach to edge detection in noisy images. In *IEEE Transactions on Circuits and Systems I: Fundamentals, Theory and Applications*, volume 46, pages 686–699, 1999.

[3] R. N. Czerwinski, D. L. Jones, and W. D. O'Brien. An approach to boundary detection in ultrasound imaging. In *IEEE Ultrasonic Symposium*, volume 2, pages 951–955, 1993.

[4] P. M. Novotny, J. W. Cannon, and R. H. Howe. Tool localization in 3D ultrasound images. In *Proceedings of Medical Image Computing and Computer-Assisted Intervention*, volume 2879, pages 969–970. Springer-Verlang, Berlin, 2003.

[5] M. Ding, H. N. Cardinal, W. Guan, and A. Fenster. Automatic needle segmentation in 3D ultrasound images. In *Proceedings of SPIE*, volume 4681, pages 65–76. International Society for Optical Engineering, May 2002.

[6] L. Tao, U. Castellani, A. Fusiello, and V. Murino. 3D acoustic image segmentation by a RANSAC-based approach. In *Proceedings of Oceans 2003 Marine Technology and Ocean Science Conference, San Diego, USA*, pages 1098–1101, September 2003.

[7] M. A. Fischler and R. C. Bolles. Random sample consensus: A paradigm for model fitting with applications to image analysis and automated cartography. *CACM*, 24(6):381–395, June 1981.

[8] O. Chum and J. Matas. Randomized RANSAC with T(d,d) test. In *Proceedings of the British Machine Vision Conference, Cardiff, UK*, pages 448–457, 2002.

[9] J. C. Bamber and R. J. Dickinson. Ultrasonic B-scanning: a computer simulation. *Physics in Medicine and Biology*, 25:463–479, 1980.

[10] I. Dydenko. Dynamic segmentation in ultrasound radiofrequency echocardiography. PhD Thesis, Institut National des Sciences Appliquées de Lyon, October 2003.

ISSN: 1727-1983